NeuroImage 121 (2015) 126–135

Contents lists available at ScienceDirect

NeuroImage

journal homepage: www.elsevier.com/locate/ynimg

Mapping of brain macromolecules and their use for spectral processing of ^{1}H-MRSI data with an ultra-short acquisition delay at 7 T☆

Michal Považan [a,b], Gilbert Hangel [a], Bernhard Strasser [a], Stephan Gruber [a], Marek Chmelik [a,b], Siegfried Trattnig [a,b], Wolfgang Bogner [a,*]

[a] High Field MR Center, Department of Biomedical Imaging and Image-guided Therapy, Medical University of Vienna, Vienna, Austria
[b] Christian Doppler Laboratory for Clinical Molecular MR Imaging, Vienna, Austria

ARTICLE INFO

Article history:
Received 21 April 2015
Accepted 12 July 2015
Available online 22 July 2015

Keywords:
Macromolecules
Double-inversion recovery
Human brain
7 T
Magnetic resonance spectroscopic imaging
Ultra-short acquisition delay

ABSTRACT

Long echo time (TE) MR spectroscopy (MRS) sequences are sensitive only to metabolites of low molecular weight. At shorter TE, significantly more metabolite signals are detectable, including broad signals of high-molecular-weight macromolecules (MMs). Although the presence of MM resonances can bias metabolite quantification at short TE, proper quantification of MMs is important since MMs themselves may serve as potentially valuable biomarkers for many pathologies.

We have therefore developed an FID-based 2D-MR Spectroscopic Imaging (2D-MRSI) sequence to map MMs in healthy brain tissue at 7 T within a scan time of ~17 min and a repetition time of 879 ms. This 2D-MRSI technique provides MM maps over a whole slice (i.e., including cortical gray matter) at an ultra-short acquisition delay of 1.3 ms, using double inversion for efficient nulling of low-molecular-weight metabolites.

The optimal sequence parameters were estimated using Bloch simulations, phantom testing, and *in vivo* validation. The acquired *in vivo* MM spectra ($n = 6$) included nine distinct MM peaks in the range of ~0.9–3.7 ppm. The measured average MM spectrum was incorporated into the LCModel basis set and utilized for further quantification of MRSI data sets without metabolite nulling, which were acquired in five additional volunteers. The quantification results for two basis sets, one including the MMs and one without MM spectrum, were compared.

Due to the high spectral resolution and full signal detection provided by the FID-MRSI sequence, we could successfully map five important brain metabolites. Most quantified metabolite signal amplitudes were significantly lower since the inclusion of MMs into the basis set corrected the overestimation of metabolite signals. The precision of fit (i.e., Cramér Rao lower bounds) remained unchanged. Our MM maps show that the overall MM contribution was higher in gray matter than in white matter.

In conclusion, the acquired MM spectrum improved the accuracy of metabolite quantification and allowed the acquisition of high spatial resolution maps of five major brain metabolites and also MMs.

Introduction

Proton magnetic resonance spectroscopy (^{1}H-MRS) is a versatile tool to assess metabolite levels *in vivo*. In the brain, significant changes in metabolite signals have been detected non-invasively by ^{1}H-MRS in various diseases (Howe and Opstad, 2003; Jessen et al., 2009; Kantarci et al., 2004). The advent of ultra-high-field MR scanners (i.e., ≥7 T) has led to an increase of spectral resolution and signal-to-noise ratio (SNR), thus allowing the quantification of more metabolites than at lower static magnetic field strengths (B_0) (Tkáč et al., 2009), unless special editing (Bogner et al., 2014) or 2D-MRS techniques are being used (Thomas et al., 2001). This offers a more comprehensive neurochemical profile of pathologic conditions.

With increasing B_0, there has been a trend toward MRS sequences with shorter echo times (TE). The reason for this is two-fold. On the one hand, the use of short-TE MRS sequences prevents excessive SNR loss, particularly that caused by faster T_2 relaxation at higher B_0. On the other hand, only at high B_0 it is possible to differentiate the low concentrated metabolic (often J-coupled) resonances since the spectral resolution is significantly improved (Tkáč et al., 2001). The lack of spectral resolution has long prevented the use of ultra-short-TE MRS sequences on clinical (e.g., 1.5 T) MR scanners, despite their obvious advantages, including the full detection of signal with negligible relaxation/J-coupling losses. J-coupling-related losses alone account for an ~5- to 10-fold loss in signal integral between TE ~ 0 ms and 30 ms (Xin et al., 2008).

☆ Parts of this study were presented at: Považan, M. et al., *Detection of brain macromolecules using double inversion recovery ultra-short acquisition delay ^{1}H MRSI at 7 Tesla (talk #991)*. ISMRM, 2015. Toronto.

* Corresponding author at: Lazarettgasse 14, 1090 Wien, Vienna, Austria. Fax: +43 1 40400 64750.
E-mail address: wolfgang.bogner@meduniwien.ac.at (W. Bogner).

http://dx.doi.org/10.1016/j.neuroimage.2015.07.042

Therefore, recently developed ultra-short TE or acquisition delay (TE*) sequences (Bogner et al., 2012; Henning et al., 2009) particularly enhance the detection of J-coupled metabolites, such as glutamate or myo-inositol.

In addition to the improved detection of common brain metabolites with low molecular weight, ultra-short TE/TE* sequences also provide increased sensitivity for high-molecular-weight macromolecules (MM) (Behar et al., 1994) that are often neglected during quantification. This MM contribution is more pronounced at ultra-high B_0 due to increased spectral dispersion of the MM components. Several broad MM peaks in the frequency range 0.9–4.0 ppm overlap with metabolite peaks, thus making the accurate quantification of ^{1}H-spectra challenging (Cudalbu et al., 2009) but, at the same time, offering the opportunity to study MM changes in various pathologies (Seeger et al., 2003).

The rationales for the study of brain MMs are two-fold. First, the quantification of MMs, *per se,* is of interest. Increased levels of specific MM peaks have been reported at 1.5 T in multiple sclerosis (Mader et al., 2001; Seeger et al., 2003), stroke (Graham et al., 2001; Hwang et al., 1996; Saunders et al., 1997), and brain tumors (Seeger et al., 2003). Thus, MMs may serve as potential biomarkers for multiple brain pathologies. Preliminary studies on regional, gray matter (GM)/white matter (WM) tissue, and age variations in the MM levels of healthy volunteers have been reported using single-voxel spectroscopy (SVS) (Hofmann et al., 2001; Mader et al., 2002; Schaller et al., 2014). Yet non-pathologic MM distributions in the healthy brain must be accurately assessed (i.e., using ^{1}H-MRS imaging (^{1}H-MRSI)) before pathologic MM alterations can be identified.

Second, for accurate quantification of metabolites, MM contributions must be properly estimated. Otherwise, the quantified metabolite concentrations may be erroneous (Cudalbu et al., 2012). Several methods that can account for MM signals exist: (a) mathematical estimation of MMs (Cudalbu et al., 2009), (b) direct acquisition of MM–free spectra (Knight-Scott, 1999), and (c) the incorporation of MM spectra measured in the same subject into quantification prior knowledge (Schaller et al., 2014). The mathematical estimation seems sufficiently accurate for lower B_0 (Schaller et al., 2013) but has limitations at ultra-high B_0 (Cudalbu et al., 2009). Therefore, adequate handling of MM at $B_0 \geq 7$ T should be targeted, either by subtracting the MM background of spectra (b) or by adding MMs to the fitting prior knowledge (c).

The biochemical background of MMs is not fully understood, but most of the peaks may be assigned to the methyl and methylene resonances of the amino acids of cytosolic proteins (Behar and Ogino, 1993). Common properties of all MM resonances are shorter T_1 and T_2 relaxation times compared to other metabolites. In particular, the faster T_1 relaxation allows the selective detection of MMs using inversion recovery (IR)-based sequences via metabolite signal suppression (Mader et al., 2001). Traditional single inversion recovery (SIR) techniques work well with long repetition times (TR), most notably if the B_1^+ inhomogeneity over the volume of interest (VOI) is negligible. The situation is more complicated when spatially variable excitation flip angles, combined with short TR, cause position-dependent saturation behavior. This causes inversion times (TI) for optimal metabolite suppression to be spatially dependent, which induces substantial problems with larger VOIs, such as in ^{1}H-MRSI. Double-inversion recovery (DIR, i.e., adding a second inversion pulse) provides superior nulling efficiency, as it makes the saturation behavior insensitive to B_1^+ inhomogeneities (de Graaf et al., 2006).

Several groups have investigated the human MM resonances for ultra-short TE using SVS. However, these studies were still carried out with TEs > 10 ms and long TR (Penner and Bartha, 2014; Schaller et al., 2014; Snoussi et al., 2014). Further shortening of TEs would increase the SNR, but due to hardware limitations of clinical MR scanners, it is not feasible for SVS.

Therefore, in the present study, we adapted a free induction decay (FID)-based ^{1}H-MRSI sequence to measure MM signal distributions in the human brain via DIR-based nulling of metabolites with ultra-short TE* at 7 T. The acquired average MM spectrum was used as prior knowledge for a more accurate spectral quantification.

Materials and methods

Sequence design for metabolite nulling

The spectroscopic data were acquired with an FID-based, two-dimensional (2D)-MRSI sequence (Bogner et al., 2012) preceded by an additional DIR module. Two IR pulses (i.e., 10th-order WURST pulses) were implemented prior to the excitation pulse to obtain metabolite-nulled spectra (Fig. 1). The inversion time TI_1 was defined as the time interval from the center of the first inversion pulse to the center of the second inversion pulse, while the inversion time TI_2 was defined as the time interval from the center of the second inversion pulse to the center of the excitation pulse. The duration of both pulses was 40 ms with a 2000 Hz bandwidth. Repetition time (TR) was defined as the time from the center of the excitation pulse to the center of the first inversion pulse of the next cycle and includes the duration of the ADC readout. Therefore, the total duration of one repetition was $TR_{tot} = TI_1 + TI_2 + TR$ (see Fig. 1). Such definition of TR and TR_{tot} was used to keep saturation effects constant in double-inversion recovery experiment. The pulse power levels were calibrated manually by increasing the RF power until the adiabatic conditions were fulfilled. An optimized four-pulse WET scheme was used for water suppression and placed in between the inversion pulses (Ogg et al., 1994).

Simulations and experimental validation

Prior to measurements, simulations were performed to predict the optimal TI_1 values based on iteratively solving the Bloch equations for different MRSI sequence parameter settings (i.e., TR, TI_1, TI_2). TR and TI_2 were kept as short as possible to reduce the total measurement time with regards to specific absorption rate limits.

T_1 and T_2 relaxation times for these simulations were those from previous studies (Penner and Bartha, 2014; Xin et al., 2013). The steady-state behavior of longitudinal and transversal magnetization was simulated for MMs and five major metabolites, *N*-acetyl aspartate (NAA), creatine (Cr), choline (Cho), glutamate (Glu), and myo-inositol (Ins), over a TR range of 600–1200 ms, as well as a TI_1 of 300–1000 ms, and a TI_2 ranging from 10 to 150 ms. The transversal magnetization for SIR and DIR was simulated to compare both approaches.

To test the simulation results, several phantom measurements were performed with different flip angles, TI_1s, and TI_2s; obtained spectra were quantified and compared to simulation output. We used a custom-made spherical phantom with a diameter of 16 cm that was filled with brain metabolites (NAA, Cr, Cho, Glu, Lactate) in a phosphate-buffered solution at physiological pH and concentration. T_1 similar to gray matter was achieved by dilution of gadolinium-containing agent in the solution.

In order to validate the simulation model and to test the behavior of MMs *in vivo*, two of the volunteers underwent six MRSI measurements in one session using different inversion times (TI_1 = 300, 400, 500, 570, 600, 700 ms) and a fixed TI_2 of 21 ms.

Subjects

Data were acquired from twelve volunteers (eight males, four females; age, 30 ± 4 years) who had no history of any brain disease on a 7 T whole-body MR scanner (Magnetom, Siemens Healthcare, Erlangen, Germany). One data set (male) was excluded due to motion artifacts. All measurements were performed using a 32-channel receive coil array combined with a volume transmit coil (Nova Medical, Wilmington, MA, USA). The study was approved by the Institutional Review Board and written informed consent was obtained from all volunteers.

Data acquisition

Based on previous simulations, the following data were acquired from all volunteers with optimized suppression of metabolite signals.

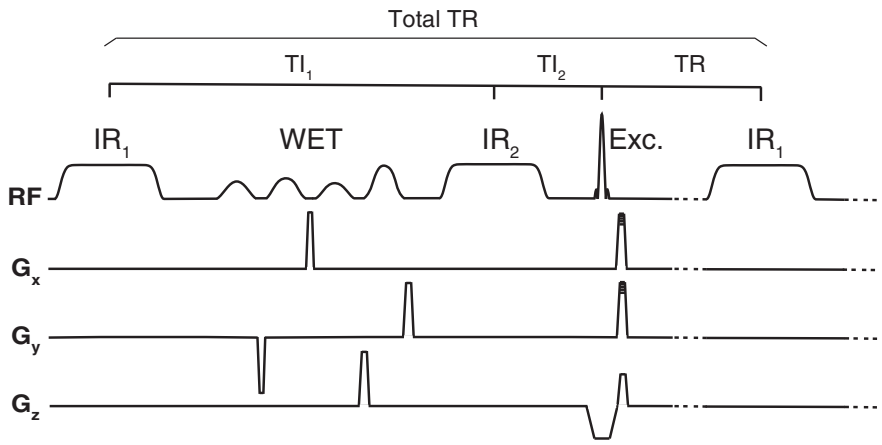

Fig. 1. Scheme of the double-inversion recovery ^{1}H-MRSI sequence with interleaved WET water suppression. Two 10th-order WURST pulses and the excitation pulse were separated by the intervals TI_1 and TI_2. TI_1 was defined as the interval from the center of the first inversion pulse to the center of the second inversion pulse. TI_2 was defined as the interval from the center of the second inversion pulse to the center of the excitation pulse. TR was defined as the time from the center of the excitation pulse to the center of the first inversion pulse of the next cycle. Thus, a total duration of one repetition was $TR_{tot} = TI_1 + TI_2 + TR$.

Prior to the actual MRSI scan, a 3D T_1-weighted, magnetization-prepared, rapid acquisition gradient echo sequence (MP2RAGE) (Marques et al., 2010) was acquired for localization purposes. Subsequently, a B_1^+-map was acquired with a pre-saturation, turbo-FLASH-based B_1^+ mapping sequence (Chung et al., 2010; Klose, 1992) at the same position as the MRSI slice. The slice was positioned parallel to the anterior commissure–posterior commissure (AC–PC) line superior to the lateral ventricles in the centrum semiovale region (Fig. 2). B_0 homogeneity was optimized using standard, second-order, field map-based shimming.

The applied *in vivo* MRSI parameters were as follows: TR, 879 ms; TE*, 1.3 ms; TI_1, 570 ms; TI_2, 21 ms; flip angle, 55°; field of view (FoV), 180 × 180 mm^2; matrix size, 32 × 32; slice thickness, 12 mm; nominal voxel size, 5.6 × 5.6 × 12 mm^3; 2048 complex spectral data points; acquisition bandwidth, 3000 Hz oversampled by a factor of 2 to 6000 Hz; one average with an elliptically sampled k-space acquired in a pseudo-spiral pattern; four dummy scans; WET water suppression with 40 ms pulse duration (four pulses) and an 80 Hz pulse bandwidth (Ogg et al., 1994); and scan time ~17 min.

Five additional data sets were measured without inversion recovery (non-DIR) using a two-dimensional, FID-based MRSI sequence (Bogner et al., 2012). The sequence parameters were identical except for the following: TR, 600 ms; flip angle, 45°; FoV, 220 × 220 mm^2; matrix size, 64 × 64; nominal voxel size, 3.4 × 3.4 × 12 mm^3; and scan time, ~30 min.

Spectral processing of MM basis set

To obtain a metabolite- and artifact-free MM spectrum from all subjects, the following steps were taken. A custom script written in Matlab (version R2009a; The MathWorks, Inc., Natick, MA) and Bash (version 4.2.25, Free Software Foundation, Boston, MA) was used for automated,

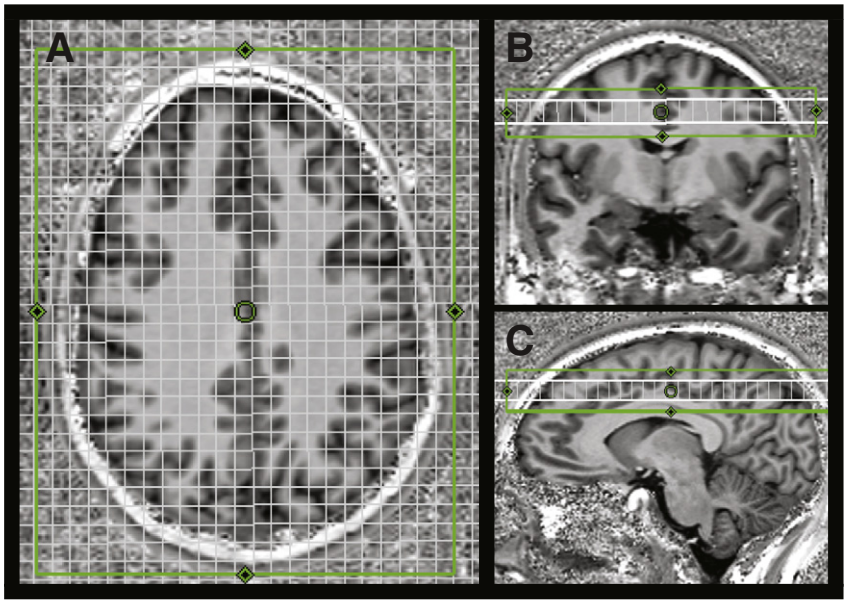

Fig. 2. (A) Axial, (B) coronal, and (C) sagittal views of the double-inversion recovery MRSI slice (32 × 32 matrix) positioned on a T_1-weighted image. The green box indicates the shim volume used for the MRSI measurement.

user-unbiased post-processing of the raw data (Považan et al., 2014), which were first coil-combined and automatically phase corrected using MUSICAL (Strasser et al., 2013). Only spectra within a brain mask, which was derived from the high-resolution T_1-weighted image (Smith, 2002), were processed. In order to decrease peripheral lipid contamination, the data sets were Hamming filtered. A region of interest (ROI) that included 10 × 11 voxels in the central part of the slice was defined. Spectra from this ROI were exported to jMRUI 3.0 (Naressi et al., 2001), frequency aligned to correct for B_0 inhomogeneities, and summed to increase the SNR. The residual water peak was removed using Hankel-Lanczos Singular Value Decomposition (HLSVD). Using a TE* of 1.3 ms introduced a small first-order phase error during data acquisition. For visual and practical purposes, this error was corrected in jMRUI and later reintroduced prior to inclusion into the LCModel basis set. To obtain metabolite-free MM spectra, the Advanced Method for Accurate, Robust, and Efficient Spectral fitting (AMARES; Vanhamme et al., 1997) was used to remove any remaining metabolite signals, as described by Craveiro et al. (2014). A single MM spectrum consisting of a signal from GM and WM was obtained for every volunteer. As the spectral resolution of the data acquired from different volunteers was equally good, it was possible to sum the acquired MM spectra of all volunteers. Thus, an average *in vivo* MM spectrum was obtained.

Metabolite quantification with the MM basis set

To determine the influence of adding an MM spectrum to the metabolite quantification, the average *in vivo* MM spectrum of six volunteers was included into an LCModel basis set (Fig. 3) consisting of 17 metabolite resonances, as simulated in NMR SCOPE (jMRUI 5.0): α-glucose (Glc), aspartate (Asp), total choline (tCho) [glycerophosphorylcholine (GPC) + phosphorylcholine (PCh)], total creatine (tCr) [phosphocreatine (PCr) + Cr], γ-aminobutyric acid (GABA), Glu, glutamine (Gln), glutathione (GSH), glycine (Gly), lactate (Lac), Ins, NAA, *N*-acetylaspartyl glutamate (NAAG), scyllo-inositol (Scyllo), and taurine (Tau). Pulse simulations were performed using one hard pulse and FID acquisition consisting of 32 768 time points with 0.0333 ms readout dwell time. Total duration in time domain was 1090.9 ms.

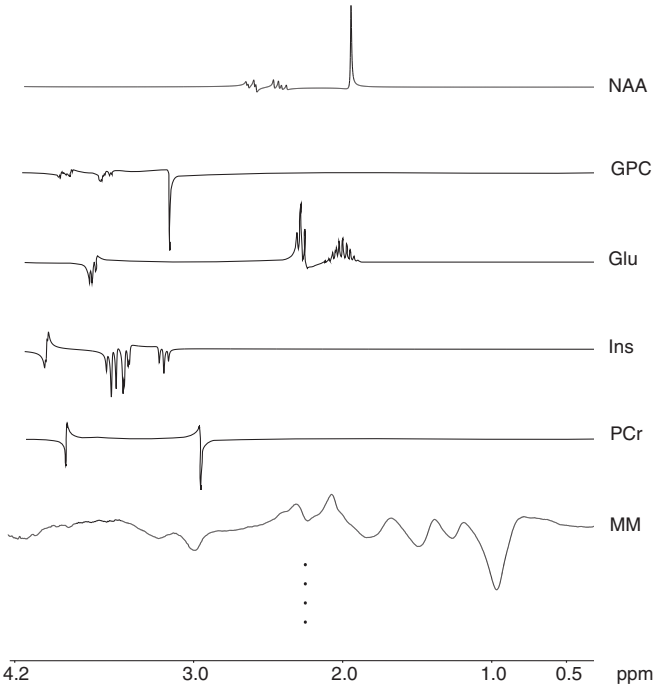

Fig. 3. LCModel basis set with a few major metabolite resonances displayed together with the MM spectrum. For LCModel quantification, all 17 metabolites were used, as stated in Section 2.6. Note that the first-order phase of the simulated spectra matches the phase of the measured data.

To take the first-order phase error due to the TE* into account, the first 39 points of all basis set FIDs were removed, which enabled the spectral fitting of signal intensities even if the phase of the spectrum was negative (Bogner et al., 2012; Henning et al., 2009). The same first-order error was reintroduced to the previously obtained average *in vivo* MM spectrum.

The five non-DIR MRSI data sets were quantified twice using LCModel 6.3 (Provencher, 2001). For the first LCModel processing cycle, the applied basis set did not account for MM, while for the second LCModel processing cycle, the averaged *in vivo* MM spectrum was included. MM peaks as provided by LCModel were omitted from the basis sets because they did not possess the first-order error. The frequency range considered for the first cycle was 1.8–4.2 ppm, whereas the second cycle was analyzed from 0.5 to 4.2 ppm to fit all major MM resonances.

Maps that visualized the distribution of MMs and brain metabolites of all healthy volunteers were displayed using MINC (MINC tools; v2.0; McConnell Brain Imaging Center, Montreal, Canada). All data with CRLB values >20% and line widths >22 Hz were excluded from visualization and further evaluation.

Evaluation

The metabolite levels and CRLBs obtained from the first and the second LCModel processing cycle of non-DIR data sets were compared voxel-wise, using a Student's paired *t*-test. The *p*-values under 0.01 were considered statistically significant. GM and WM regions were compared separately. The mean difference in signal intensities and CRLBs of NAA, tCho, tCr, Ins, and Glu were obtained by averaging over all voxels in the GM/WM region for each subject. Subsequently, these values were averaged over all subjects. Only metabolites that could be reliably quantified over the whole slice and both in GM and WM in all volunteers were considered for statistical analysis.

Results

Simulations and validations

Our Bloch simulations predicted an optimal nulling of metabolite signals for an inversion time TI_1 of 570 ms (assuming a fixed TI_2 of 21 ms and TR time of 879 ms, both as short as possible). For this sequence timing, the simulated signals of NAA, Cr (3 ppm), Cho, Ins, and Glu were below 5% of the full signal (without inversion). The residual signal of Cr (4 ppm) was 8% due to its faster T_1 relaxation. Simulations showed 53% remaining MM signal for SIR compared to 50% for the DIR nulling method. Phantom measurements confirmed the simulated values. The *in vivo* DIR experiment performed in two volunteers provided additional support for the simulation model, in which the time course of individual signals was observed (Fig. 4). The smallest metabolic residuals were achieved when the TI_1 was set to 570 ms.

Spectral processing of the MM basis set

The summed metabolite-nulled spectra of all six volunteers were consistent and provided evidence of the high spectral quality over the whole frequency range from 0.5 to 4.2 ppm without extracerebral lipid contamination. Small metabolite residuals were observed in all MM spectra in accordance with simulations. The residuals of NAA (2.01 ppm), Ins (3.52 ppm), Glu (2.3 ppm), Gln (2.45 ppm), and tCr (3.98 ppm) were efficiently removed from all metabolite-nulled spectra. The FWHM of MM1 (0.89 ppm) over all six volunteers was 38.1 Hz ± 0.1

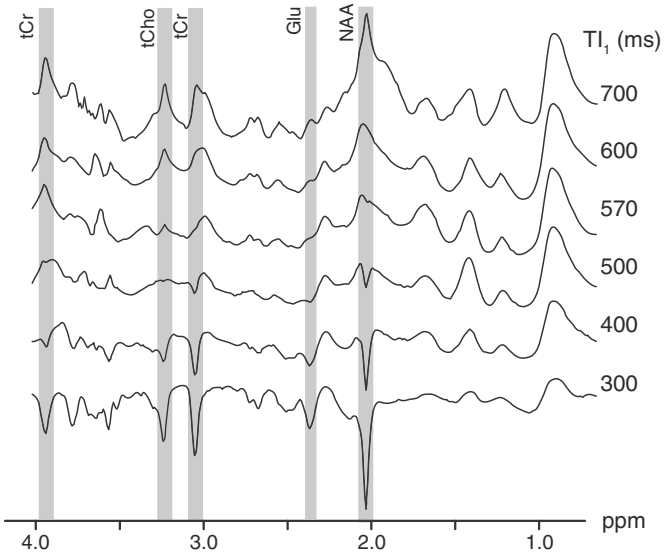

Fig. 4. Series of *in vivo* double-inversion recovery ^{1}H-MR spectra acquired with fixed $TI_2 = 21$ ms and variable TI_1 (from 300 ms to 700 ms) to determine the optimal timing to null the metabolites. Data were acquired from one volunteer, but each spectrum is actually a sum of 110 frequency-aligned spectra (i.e., 10×11 voxels) from a rectangular region of interest located in the centrum semiovale region of brain. Since the spectra are acquired with an acquisition delay, first-order phase correction was applied. The optimum for minimizing the metabolite signals was found at TI_1 of 570 ms.

(mean ± SD). Thus, the variation of the FWHM was small enough to allow simple averaging of the MM spectrum obtained from all six volunteers (Fig. 5).

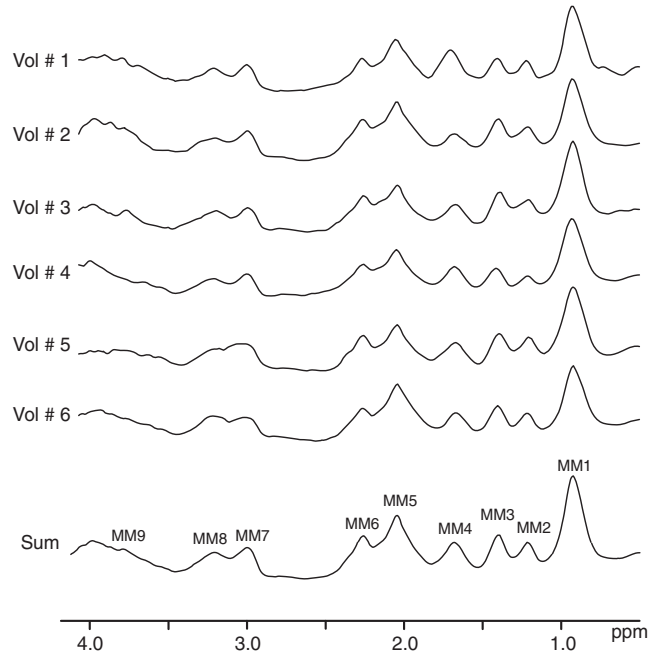

Fig. 5. A set of MM signals acquired from six healthy volunteers and a sum of these signals. Spectra were first-order phase corrected, and all metabolite residuals were removed using jMRUI 5.0. Nine distinct MM resonances were detected at the following frequency positions: 0.91 ppm (MM1), 1.21 ppm (MM2), 1.43 ppm (MM3), 1.67 ppm (MM4), 2.04 ppm (MM5), 2.26 ppm (MM6), 2.99 ppm (MM7), 3.21 ppm (MM8), and 3.77 ppm (MM9).

Metabolite quantification with the MM basis set

Basis set comparison

When comparing the quantification results obtained from five non-DIR 2D-MRSI data sets, processed with/without the inclusion of an MM spectrum into the LCModel basis set, there were two major findings:

After the inclusion of MM in the basis set, the metabolite signals were significantly smaller ($p < 0.001$) for most quantified metabolites (Fig. 6A). The differences are summarized in Table 1.

The fitting precision (i.e., CRLBs provided by the LCModel) remained unchanged ($p < 0.005$) (Table 2).

Regional differences

MM differences (i.e., quantified MM signal from the 0.5 to 4.2 ppm region) were found between GM and WM, with higher signal in the GM regions (Figs. 7A and 8).

In addition, we also found regional and GM/WM differences in other metabolites (Figs. 7A, 8, and 9). Representative spectra from GM and WM regions are shown (Figs. 7B and C), together with an overall fit and the fitted MM spectrum. The tCr signal was higher in GM than in WM regions, whereas tCho was higher in the central WM region. Glu exhibited a lower signal intensity in WM. NAA and GSH were relatively evenly distributed throughout the measured brain slice.

Discussion

In our study, we mapped the MM overall signal in the human brain *in vivo* using a 2D ^{1}H-MRSI FID-based sequence with an ultra-short TE* and DIR-based metabolite nulling at 7 T. The parameters were optimized by simulation and validated by a set of *in vitro* and *in vivo* tests. The average MM spectrum of six volunteers was incorporated into the LCModel basis set to account for spectral MM contributions during metabolic quantification of non-DIR spectra. The use of this improved fitting prior knowledge allowed the high-resolution mapping of regional differences in MMs. Our approach removed the overestimation of metabolite signals that is present when a solely spline baseline is used. Thus, the quantification accuracy was improved, whereas the quantification precision (i.e., CRLBs) remained unchanged.

Double-inversion recovery

SIR is usually the method of choice for metabolite nulling. However, the situation is different at ultra-high fields and sequences with very short TR. The use of spatially variable excitation flip angles, combined with a short TR, leads to spatially dependent saturation effects. These saturation effects themselves affect the ideal TI for perfect nulling of metabolite signals. Moreover, not using a 90° excitation leads to signal loss. DIR improves the nulling efficiency, as it is insensitive to B_1^+ inhomogeneities. DIR provides improved suppression of metabolite resonances (de Graaf et al., 2006) with no significant difference in the remaining MM signal amplitude. However, DIR can introduce stronger T_1 weighting to the MM resonances compared to SIR (de Graaf et al., 2006), which is a disadvantage for long-TR sequences. Nevertheless, the use of MM spectra acquired via DIR might be advantageous when used to quantify short-TR spectra. In our study, we did not observe any changes in fitting quality (CRLBs) when the measured MM spectrum was included in the LCModel basis set.

MM acquisition

In order to increase the SNR of our acquired MM signal, MM spectra obtained from the central part of the brain were summed after visual inspection for spectral quality and after frequency correction. Although a difference in the MM spectrum between WM and GM was reported, it has been suggested that a general MM spectrum that does not distinguish

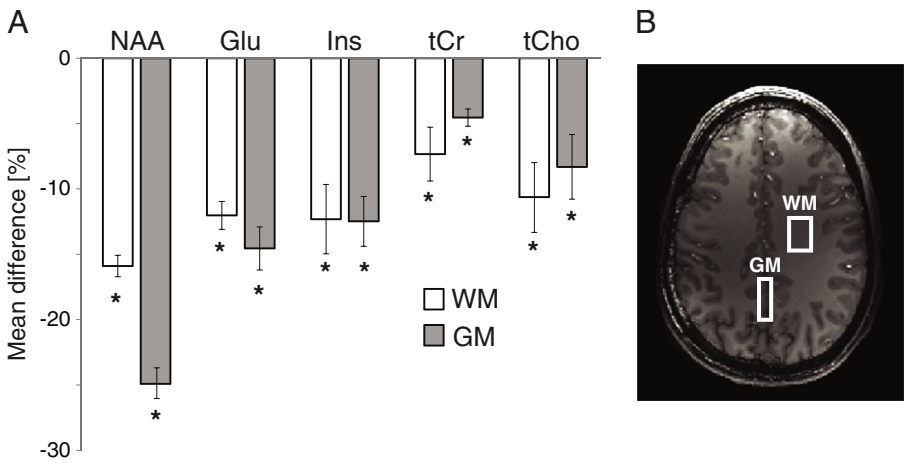

Fig. 6. (A) Mean signal intensity difference (mean ± SE) between the first and second LCModel processing cycle obtained in the WM and in the GM of five volunteers. During the first processing cycle, a basis set without MM spectrum was used, whereas in the second cycle, the same basis set plus the average MM spectrum was used for spectral fitting. A significant decrease of metabolic concentrations (*statistical significance, $p < 0.001$) was observed for NAA, Glu, Ins, tCr, and tCho in both the GM and WM regions for cycle two. (B) The position of the investigated WM (6 × 4 voxels) and GM (8 × 3 voxels) regions of interest are indicated by white rectangular boxes.

between GM and WM contributions is sufficient for reliable metabolite quantification in the healthy human brain (Schaller et al., 2014). In accordance with that observation, we used a summed MM signal that originated from both WM and GM regions. The variations in the MM spectrum between volunteers were not considered significant (i.e., the full width at half maximum of the MM resonance at 0.9 ppm (MM1) was tested between subjects). The line widths observed for the MM1 resonance (~38 Hz) were comparable to those previously observed at 7 T (~43 Hz) (Snoussi et al., 2014). We found modest differences in the MM2 and MM4 resonances and in the frequency region from 3.5 to 4.2 ppm. These differences could be explained by different contributions of GM and WM volume covered by the summed voxels and were neglected as recently proposed (Schaller et al., 2014). The proper definition of the prior knowledge on frequency, line width, phase, and amplitude in AMARES algorithm ensured that a precise and robust removal of residual metabolite peaks was achieved, while avoiding the over- or underestimation of the MM spectrum.

Summing the MM spectrum that was obtained from several voxels in a specified ROI led to an improved SNR without degradation of spectral resolution. Ding et al. (2014) showed that the line widths after summing several frequency-aligned MRSI voxels over a specified ROI were significantly smaller than the line widths of spectra obtained by SVS from the same ROI. This indicates that MRSI should be favored over SVS, if larger ROIs are needed to reliably detect a metabolite. However, the *a priori* better SNR of SVS should be considered (Zhang et al., 2012).

Other MM detection approaches

To the best of our knowledge, only two studies at a lower field-strength (i.e., 2.1 T) were published about how the MM signal should be handled when using MRSI. Hwang et al. (1996) detected MM in healthy volunteers and patients with subacute stroke, and Graham et al. (2001) focused solely on stroke patients. Metabolic maps of two major MM peaks (i.e., 0.9 ppm and 2.05 ppm) from healthy subjects and of the 1.3 ppm resonance for patients were presented. However, the echo time was >20 ms, and the long measurement time and low resolution hampered wider clinical application. Moreover, the signal at 1.3 ppm was mostly assigned to lipids, and not MMs, as noted in recent studies (Balchandani and Spielman, 2008). Thus, an actual change in MM resonances, as defined by Behar et al. (1994) in diseased tissue, was reported solely in SVS studies (Mader et al., 2002; Seeger et al., 2003).

To our knowledge, MMs have not yet been measured with a TE/TE* as short as that presented in our study. Human studies targeting MMs with SVS methods (i.e., STEAM, SPECIAL, or semi-LASER localization) have used TEs ranging from 38 ms down to 12 ms and substantially longer TRs of several seconds than those used in our study (Mader et al., 2002; Penner and Bartha, 2014; Seeger et al., 2001; Schaller et al., 2013). Even animal studies reached TEs no shorter than 2.8 ms (Craveiro et al., 2014; Cudalbu et al., 2009).

Metabolic maps

The spatial distribution and concentration differences between GM/WM were overall in good agreement with previous studies (Baker et al., 2008; Bogner et al., 2012; Degaonkar et al., 2005; Emir et al., 2012; Henning et al., 2009). Five major metabolites (NAA, tCr, tCho, Ins, Glu + Gln) together with overall signal of MM fulfilled the quality assurance criteria over the whole slice in all volunteers.

Table 1
Mean metabolite signal intensity difference between the data set quantified with and without MM included in the basis set. A decrease of all major metabolite signals was observed. The mean signal intensity difference was obtained by averaging the mean signal intensity differences of individual subjects.

	Mean signal intensity difference (%) ± SE	
	WM	GM
Metabolite		
NAA	−15.9 ± 0.8	−24.9 ± 1.5
tCho	−10.6 ± 3.4	−8.3 ± 3.1
tCr	−7.3 ± 2.1	−4.5 ± 0.7
Glu	−12.0 ± 1.1	−14.6 ± 1.7
Ins	−12.3 ± 2.7	−12.5 ± 1.9

Table 2
Cramer Rao lower bounds (CRLB, mean ± SD) obtained from LCModel analysis of ^{1}H spectra from the WM region and the GM region in five volunteers (see Fig. 6B), using the basis set with and without MM spectrum (MMS) included. Five major metabolites were chosen for the analysis.

	CRLB (%) ± SD			
	WM		GM	
Metabolite	With MMS	Without MMS	With MMS	Without MMS
NAA	3.7 ± 0.3	3.4 ± 0.3	3.4 ± 0.3	3.4 ± 0.3
tCho	3.9 ± 0.4	5.1 ± 1.1	3.9 ± 0.1	4.5 ± 0.6
tCr	3.0 ± 0.3	3.1 ± 0.1	3.6 ± 0.4	3.9 ± 0.1
Glu	3.9 ± 0.4	3.5 ± 0.5	7.8 ± 1.1	7.6 ± 0.4
Ins	4.9 ± 0.3	4.6 ± 0.5	6.3 ± 1.3	6.1 ± 1.1

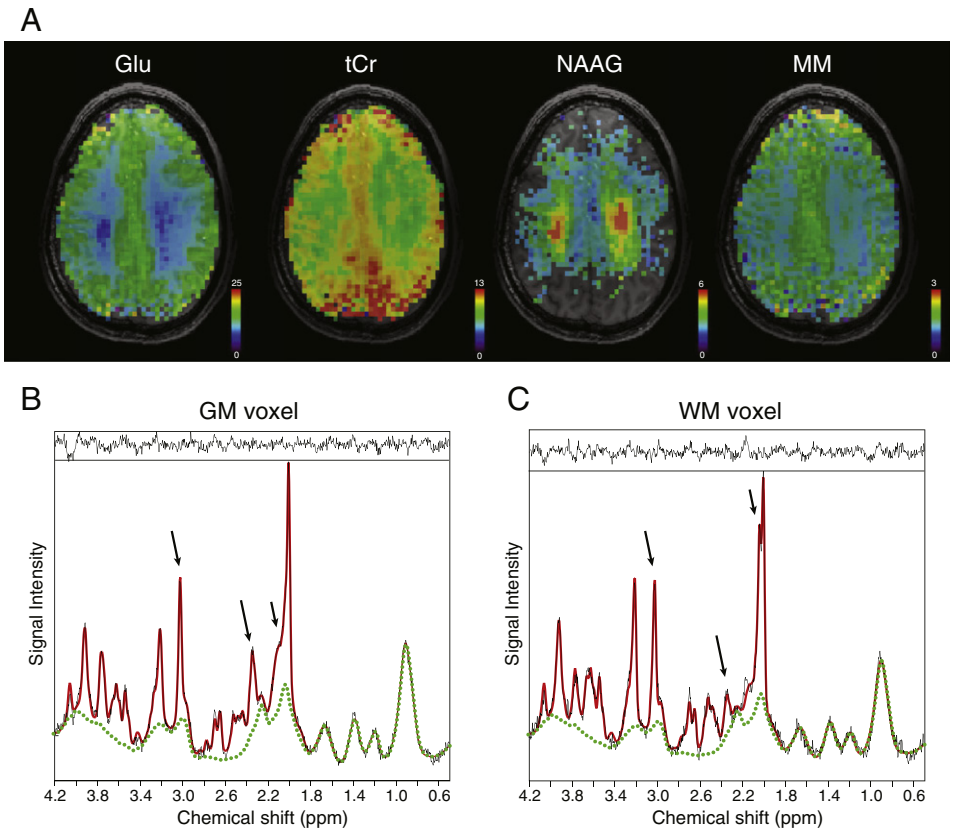

Fig. 7. (A) Metabolic maps of glutamate (Glu), total creatine (tCr), *N*-acetyl aspartyl glutamate (NAAG), and macromolecules (MM) in native 64 × 64 resolution showing the signal intensity distribution over the whole brain slice. A characteristic feature of all four metabolic maps is the difference between the GM and WM signal intensity, particularly Glu, and MM signals are decreased in the WM, whereas NAAG is increased in the mesial WM. tCr shows increased signal intensity in GM. ^{1}H-MRSI spectra (black), fit (red), fitted MM spectrum (dotted green), and fitting residuum (top) of (B) a GM voxel and (C) a WM voxel. Arrows indicate the increased signal of tCr and Glu in the GM and increased signal of NAAG in the WM. Overall, the lower MM spectrum in the WM voxel is also apparent.

Furthermore, NAAG signal was observed in the mesial part of WM and GM, whereas in cortical GM the SNR was insufficient (see Fig. 7A). A signal of GSH was observed with CRLB values below 20% in one volunteer (Fig. 8). NAA was fairly uniformly distributed over the whole slice with a slightly higher signal in the occipital GM. In contrast, the tCho signal showed greater regional differences, with lower levels in the GM, except the midline frontal GM, where the signal intensity reached the values of WM, which is in accordance with published papers (Baker et al., 2008; Degaonkar et al., 2005; Emir et al., 2012). tCr was more abundant in GM than in WM. A higher NAAG signal in mesial WM was evident (Pouwels and Frahm, 1998). Glx (i.e., Glu + Gln) levels in GM were higher than the levels in WM since Glu and Gln are found in close proximity to neuronal synapses (Baker et al., 2008; Marsman et al., 2013). In accordance with previous SVS studies, we found a higher overall MM signal in GM (especially medial GM) than in WM (Schaller et al., 2014).

MM—a potential biomarker

The proper handling of the MM signal is mandatory, not only to achieve improved neurochemical profiling but also because of the advent of fast short-TR and short-TE/TE* MRSI sequences (Boer et al., 2011; Bogner et al., 2012; Henning et al., 2009). Such sequences are particularly sensitive to high-molecular-weight resonances, such as MMs, which can bias accurate quantification. Boer et al. did not incorporate any MM estimation into their MRSI quantification routine (Boer et al., 2012). Henning et al. included a simulated MM baseline, but mathematical models of the MM baseline, such as a spline baseline, were found to be insufficient at ultra-high fields (Cudalbu et al., 2009; Pfeuffer et al., 1999). The spline baseline failed to adequately model the MM background at $B_0 \geq 7$ T, which was reflected in significant quantification differences (Cudalbu et al., 2009; Schaller et al., 2014). This is in agreement with our observations. Yet the spline baseline is the default baseline model in the LCModel. Another alternative is to use individual MM resonances present in LCModel by default. However, the introduction of first-order error is not possible, disqualifying this approach from application in pulse-acquire sequences with acquisition delay.

Therefore, to improve the metabolite quantification, the measured MM contribution should be included in the prior knowledge. This is becoming even more important at ultra-high field and short/ultra-short TE. Otherwise, an overestimation of metabolite signals occurs. Preferably, similar sequence parameters (i.e., TR, TE*, and a localization technique) should be used to acquire MM spectrum. However, the hardware and software restrictions sometimes do not allow achieving the same settings for SVS and MRSI. Hence, adapting our MRSI sequence to measure metabolite-nulled spectra was the only way to achieve these settings for such a short TE*.

One of the advantages of MRSI techniques is the possibility to create metabolic maps that reveal even subtle local changes of metabolite levels throughout the brain volume.

In our study, an additional map for the distribution of the total MM amplitude was obtained along with other metabolic maps. This enables the exploration of any regional or tissue differences for each metabolite, as well as for the MMs. This might be of clinical relevance for brain diseases, which manifest as a diffuse metabolic change over a wider tissue region rather than a focal change. To date, several studies have shown altered total MM signal or individual MM peaks in diseased brain (Graham et al., 2001; Kaiser et al., 2005; Mader et al., 2001; Opstad

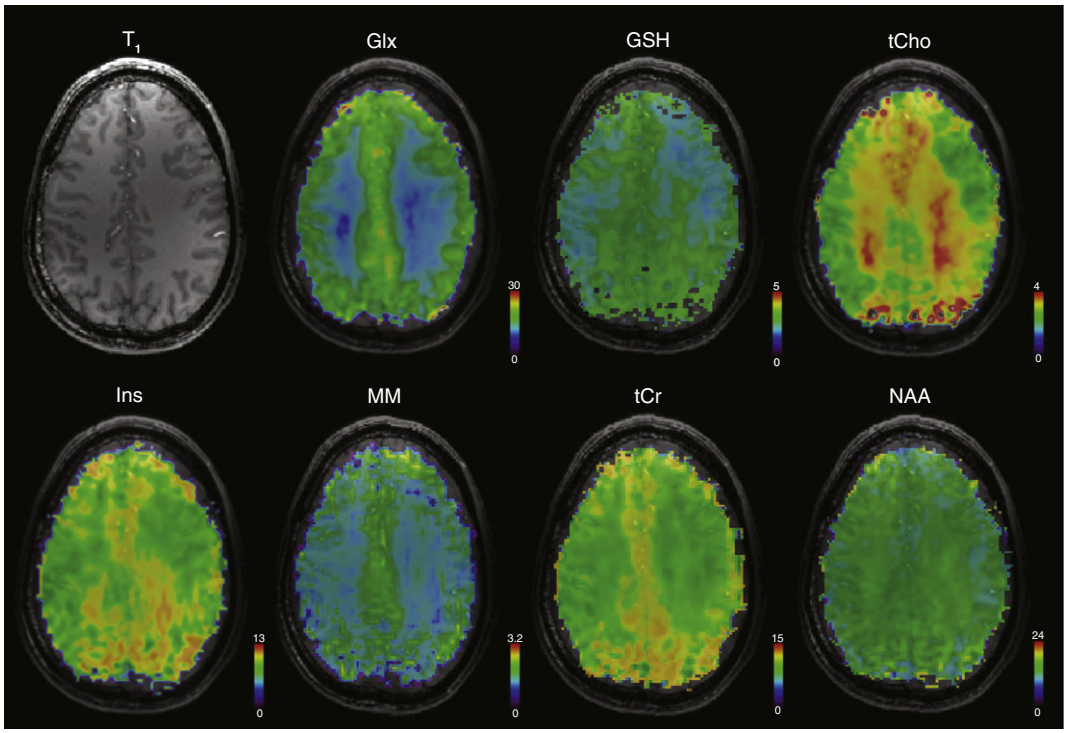

Fig. 8. T_1-weigthed image and metabolic maps of Glx (i.e., Glu + Gln), GSH, tCho, Ins, MM, tCr, and NAA resampled from 64 × 64 to 128 × 128 resolution illustrate the high spatial resolution of our metabolic maps.

et al., 2004; Seeger et al., 2003), but the changes were detected in only a small region that was restricted to a predefined VOI. Due to lower field-strength and longer TEs, the SNR loss impeded further clinical investigations. The total MM amplitude maps, as presented in our study, can support future MM studies of brain pathologies.

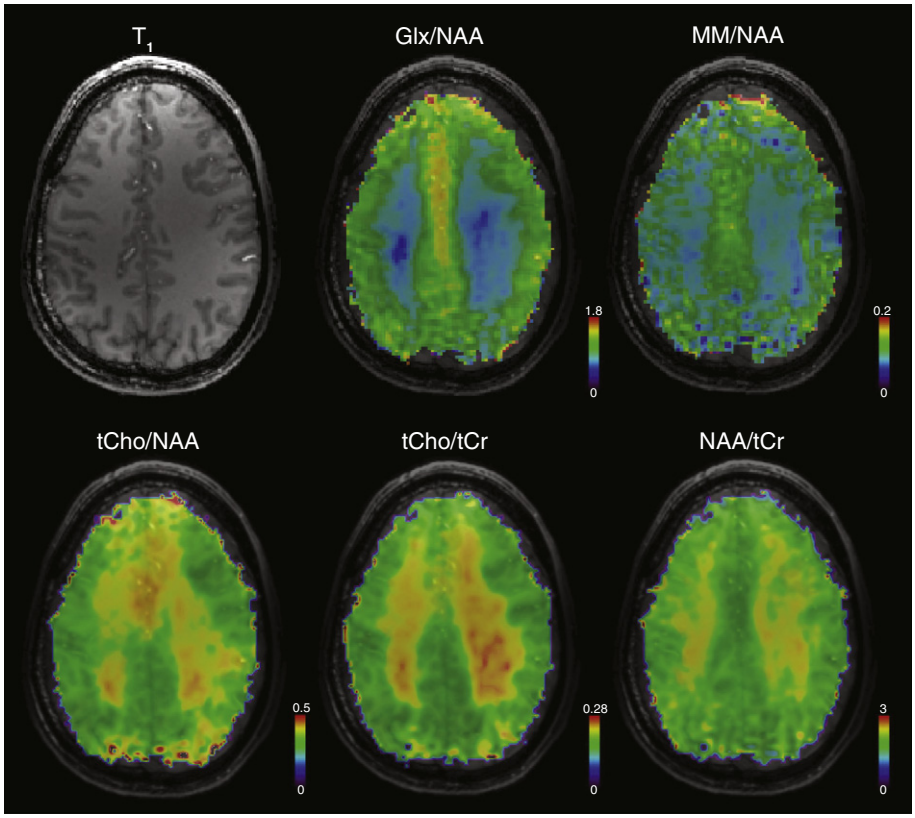

Fig. 9. T_1-weighted image and metabolic ratio maps of Glx/NAA, MM/NAA, tCho/NAA, tCho/tCr, and NAA/tCr resampled from 64 × 64 to 128 × 128 resolution.

Quality assurance

The 2D/3D-MRSI approaches that cover large parts of the brain typically acquire data of variable spectral quality, ranging from good-quality spectra to those with either low signal intensities in regions of significant CSF contribution or broadened line shapes and large lipid contamination (Maudsley et al., 2006). The demands on signal analysis are higher compared to SVS. Thus, robust spectral fitting routines and quality control should be part of the processing pipeline. Therefore, our exclusion criteria were set for CRLB and FWHM to avoid low-quality data from analysis. In addition, all data were processed using a user-independent, automated post-processing routine, which facilitated optimization of processing time and minimized user-induced systematic error.

Limitations

Since there is strong evidence that the different MM resonances are altered non-uniformly in the diseased brain, healthy MM spectrum might not be adequate to fully describe the MM contribution in spectra obtained from pathologically changed brain tissue (Craveiro et al., 2014; Graham et al., 2001; Mader et al., 2002). Possibly elevated lipid signals that are, for instance, visible in tumors or attributable to demyelination should be also considered for good quantification (Howe et al., 2003; Mlynárik et al., 2012). A possible solution would be the parameterization of the measured MM spectrum by splitting the full MM spectrum into individual components (Seeger et al., 2003).

Despite the only minor MM tissue (WM/GM) differences that we observed, the inclusion of separate WM and GM MM contribution may further increase the robustness of quantification.

Conclusion

The use of our FID-based DIR ^{1}H-MRSI sequence enabled the detection of macromolecular (i.e., metabolite-nulled) spectra in healthy human brains with a short TR and an ultra-short TE* of 1.3 ms at 7 T. Improved metabolite quantification was achieved by including the average MM spectrum in the LCModel prior knowledge. This provided not only a more accurate quantification and high-resolution mapping of common brain metabolites at 7 T but also additional maps of MM distributions over the whole slice. This could be of substantial value for future studies on the pathophysiology of major neurological and psychiatric diseases.

Acknowledgments

This study was supported by the Austrian Science Fund (FWF): KLI-61 and the FFG Bridge Early Stage grant no. 846505. We would like to thank Martin Kršňák for his valuable advice and support.

Appendix A

The combination of equations for free precession (Eq. (A.1)) and for rotation of magnetization (Eq. (A.2)) based on Bloch equations were used, considering the parameters for double inversion.

$$M(t, T_1, T_2, \theta) = A * M_0 + B \tag{A.1}$$

$$R_{xy}(\varphi) = \begin{bmatrix} \cos(\varphi) & 0 & \sin(\varphi) \\ 0 & 1 & 0 \\ -\sin(\varphi) & 0 & \cos(\varphi) \end{bmatrix} \tag{A.2}$$

where M is the magnetization at time t, t is the time interval during which the signal decays, M_0 is the initial magnetization (i.e., $t = 0$ s), T_1 and T_2 are longitudinal and transversal relaxation rates (all in seconds), θ is the angular velocity of precession, and φ is the flip angle in degrees. A and B are defined as follows (Eq. (A.3)):

$$A = \begin{bmatrix} e^{\frac{-t}{T_2}} & 0 & 0 \\ 0 & e^{\frac{-t}{T_2}} & 0 \\ 0 & 0 & e^{\frac{-t}{T_1}} \end{bmatrix} * \begin{bmatrix} \cos(\theta) & -\sin(\theta) & 0 \\ \sin(\theta) & \cos(\theta) & 0 \\ 0 & 0 & 1 \end{bmatrix} \qquad B = \begin{bmatrix} 0 \\ 0 \\ 1-e^{\frac{-t}{T_1}} \end{bmatrix} \tag{A.3}$$

These equations were implemented in MATLAB (version R2009a; The MathWorks, Inc., Natick, MA) and solved iteratively to simulate steady-state behavior. The simulations assumed relaxation times for brain metabolites at 7 T, as reported previously for T_1 (Xin et al., 2013) and for T_2 (Penner and Bartha, 2014).

Appendix B. Supplementary data

Supplementary data to this article can be found online at http://dx.doi.org/10.1016/j.neuroimage.2015.07.042.

References

Baker, E.H., Basso, G., Barker, P.B., Smith, M.A., Bonekamp, D., Horská, A., 2008. Regional apparent metabolite concentrations in young adult brain measured by ^{1}H MR spectroscopy at 3 Tesla. J. Magn. Reson. Imaging 27, 489–499. http://dx.doi.org/10.1002/jmri.21285.

Balchandani, P., Spielman, D., 2008. Fat suppression for ^{1}H MRSI at 7 T using spectrally selective adiabatic inversion recovery. Magn. Reson. Med. 59, 980–988. http://dx.doi.org/10.1002/mrm.21537.

Behar, K.L., Ogino, T., 1993. Characterization of macromolecule resonances in the ^{1}H NMR spectrum of rat brain. Magn. Reson. Med. 30, 38–44.

Behar, K.L., Rothman, D.L., Spencer, D.D., Petroff, O.A.C., 1994. Analysis of macromolecule resonances in ^{1}H NMR spectra of human brain. Magn. Reson. Med. 32, 294–302. http://dx.doi.org/10.1002/mrm.1910320304.

Boer, V.O., Klomp, D.W.J., Juchem, C., Luijten, P.R., de Graaf, R. a, 2011. Multislice ^{1}H MRSI of the human brain at 7 T using dynamic B_0 and B_1 shimming. Magn. Reson. Med. 68, 1–9. http://dx.doi.org/10.1002/mrm.23288.

Boer, V.O., van de Bank, B.L., van Vliet, G., Luijten, P.R., Klomp, D.W.J., 2012. Direct B_0 field monitoring and real-time B_0 field updating in the human breast at 7 Tesla. Magn. Reson. Med. 67, 586–591. http://dx.doi.org/10.1002/mrm.23272.

Bogner, W., Gruber, S., Trattnig, S., Chmelík, M., 2012. High resolution mapping of human brain metabolites by free induction decay ^{1}H MRSI at 7 T. NMR Biomed. 873–882 http://dx.doi.org/10.1002/nbm.1805.

Bogner, W., Gagoski, B., Hess, A.T., Bhat, H., Tisdall, M.D., van der Kouwe, A.J.W., Strasser, B., Marjańska, M., Trattnig, S., Grant, E., Rosen, B., Andronesi, O.C., 2014. 3D GABA imaging with real-time motion correction, shim update and reacquisition of adiabatic spiral MRSI. NeuroImage 103, 290–302. http://dx.doi.org/10.1016/j.neuroimage.2014.09.032.

Chung, S., Kim, D., Breton, E., Axel, L., 2010. Rapid B_1^+ mapping using a preconditioning RF pulse with TurboFLASH readout. Magn. Reson. Med. 64, 439–446. http://dx.doi.org/10.1002/mrm.22423.

Craveiro, M., Clément-Schatlo, V., Marino, D., Gruetter, R., Cudalbu, C., 2014. In vivo brain macromolecule signals in healthy and glioblastoma mouse models: ^{1}H magnetic resonance spectroscopy, post-processing and metabolite quantification at 14.1 T. J. Neurochem. 1–10 http://dx.doi.org/10.1111/jnc.12673.

Cudalbu, C., Mlynárik, V., Xin, L., Gruetter, R., 2009. Quantification of in vivo short echo-time proton magnetic resonance spectra at 14.1 T using two different approaches of modelling the macromolecule spectrum. Meas. Sci. Technol. 20, 104034. http://dx.doi.org/10.1088/0957-0233/20/10/104034.

Cudalbu, C., Mlynárik, V., Gruetter, R., 2012. Handling macromolecule signals in the quantification of the neurochemical profile. J. Alzheimers Dis. 31 (Suppl. 3), S101–S115. http://dx.doi.org/10.3233/JAD-2012-120100.

De Graaf, R. a, Brown, P.B., McIntyre, S., Nixon, T.W., Behar, K.L., Rothman, D.L., 2006. High magnetic field water and metabolite proton T_1 and T_2 relaxation in rat brain in vivo. Magn. Reson. Med. 56, 386–394. http://dx.doi.org/10.1002/mrm.20946.

Degaonkar, M.N., Pomper, M.G., Barker, P.B., 2005. Quantitative proton magnetic resonance spectroscopic imaging: regional variations in the corpus callosum and cortical gray matter. J. Magn. Reson. Imaging 22, 175–179. http://dx.doi.org/10.1002/jmri.20353.

Ding, X., Maudsley, A., Sabati, M., Sheriff, S., Lanfermann, H., 2014. Comparison of a short-TE whole brain MR spectroscopic imaging to single voxel spectroscopy for measurement of metabolite concentrations in human brain. Proc. Intl. Soc. Mag. Reson. Med.

Emir, U.E., Auerbach, E.J., Van De Moortele, P.-F., Marjańska, M., Uğurbil, K., Terpstra, M., Tkáč, I., Oz, G., 2012. Regional neurochemical profiles in the human brain measured by ^{1}H MRS at 7 T using local B_1 shimming. NMR Biomed. 25, 152–160. http://dx.doi.org/10.1002/nbm.1727.

Graham, G.D., Hwang, J.-H., Rothman, D.L., Prichard, J.W., 2001. Spectroscopic assessment of alterations in macromolecule and small-molecule metabolites in human brain after stroke. Stroke 32, 2797–2802. http://dx.doi.org/10.1161/hs1201.099414.

Henning, A., Fuchs, A., Murdoch, J.B., Boesiger, P., 2009. Slice-selective FID acquisition, localized by outer volume suppression (FIDLOVS) for ^{1}H-MRSI of the human brain at

7 T with minimal signal loss. NMR Biomed. 22, 683–696. http://dx.doi.org/10.1002/nbm.1366.

Hofmann, L., Slotboom, J., Boesch, C., Kreis, R., 2001. Characterization of the macromolecule baseline in localized ^{1}H-MR spectra of human brain. Magn. Reson. Med. 46, 855–863.

Howe, F.A., Opstad, K.S., 2003. ^{1}H MR spectroscopy of brain tumours and masses. NMR Biomed. 16, 123–131. http://dx.doi.org/10.1002/nbm.822.

Howe, F. a, Barton, S.J., Cudlip, S. a, Stubbs, M., Saunders, D.E., Murphy, M., Wilkins, P., Opstad, K.S., Doyle, V.L., McLean, M. a, Bell, B. a, Griffiths, J.R., 2003. Metabolic profiles of human brain tumors using quantitative in vivo ^{1}H magnetic resonance spectroscopy. Magn. Reson. Med. 49, 223–232. http://dx.doi.org/10.1002/mrm.10367.

Hwang, J.H., Graham, G.D., Behar, K.L., Alger, J.R., Prichard, J.W., Rothman, D.L., 1996. Short echo time proton magnetic resonance spectroscopic imaging of macromolecule and metabolite signal intensities in the human brain. Magn. Reson. Med. 35, 633–639.

Jessen, F., Gür, O., Block, W., Ende, G., Frölich, L., Hammen, T., Wiltfang, J., Kucinski, T., Jahn, H., Heun, R., Maier, W., Kölsch, H., Kornhuber, J., Träber, F., 2009. A multicenter ^{1}H-MRS study of the medial temporal lobe in AD and MCI. Neurology 72, 1735–1740. http://dx.doi.org/10.1212/WNL.0b013e3181a60a20.

Kaiser, L.G., Young, K., Soher, B.J., Weiner, M.W., 2005. Macromolecular and Lipid Contributions in Short Echo Time ^{1}H MRS at 4 Tesla : 1) Reliability in Normal Controls and 2) Comparative Study Between Amyotrophic Lateral Sclerosis Patients and Controls. Proc. Intl. Soc. Mag. Reson. Med.

Kantarci, K., Petersen, R.C., Boeve, B.F., Knopman, D.S., Tang-Wai, D.F., O'Brien, P.C., Weigand, S.D., Edland, S.D., Smith, G.E., Ivnik, R.J., Ferman, T.J., Tangalos, E.G., Jack, C.R., 2004. ^{1}H MR spectroscopy in common dementias. Neurology 63, 1393–1398. http://dx.doi.org/10.1212/01.WNL.0000141849.21256.AC.

Klose, U., 1992. Mapping of the radio frequency magnetic field with a MR snapshot FLASH technique. Med. Phys. 19, 1099–1104.

Knight-Scott, J., 1999. Application of multiple inversion recovery for suppression of macromolecule resonances in short echo time ^{1}H NMR spectroscopy of human brain. J. Magn. Reson. 140, 228–234. http://dx.doi.org/10.1006/jmre.1999.1799.

Mader, I., Seeger, U., Weissert, R., Klose, U., Naegele, T., Melms, a, Grodd, W., 2001. Proton MR spectroscopy with metabolite-nulling reveals elevated macromolecules in acute multiple sclerosis. Brain 124, 953–961.

Mader, I., Seeger, U., Karitzky, J., Erb, M., Schick, F., Klose, U., 2002. Proton magnetic resonance spectroscopy with metabolite nulling reveals regional differences of macromolecules in normal human brain. J. Magn. Reson. Imaging 16, 538–546. http://dx.doi.org/10.1002/jmri.10190.

Marques, J.P., Kober, T., Krueger, G., Van Der Zwaag, W., 2010. MP2RAGE, a self bias-field corrected sequence for improved segmentation and T_1 -mapping at high field. NeuroImage 49, 1271–1281. http://dx.doi.org/10.1016/j.neuroimage.2009.10.002.

Marsman, A., Mandl, R.C.W., van den Heuvel, M.P., Boer, V.O., Wijnen, J.P., Klomp, D.W.J., Luijten, P.R., Hilleke, E.H.P., 2013. Glutamate changes in healthy young adulthood. Eur. Neuropsychopharmacol. 23, 1484–1490. http://dx.doi.org/10.1016/j.euroneuro.2012.11.003.

Maudsley, A.A., Darkazanli, A., Alger, J.R., Hall, L.O., Schuff, N., Studholme, C., Yu, Y., Ebel, A., Frew, A., Goldgof, D., Gu, Y., Pagare, R., Rousseau, F., Sivasankaran, K., Soher, B.J., Weber, P., Young, K., Zhu, X., 2006. Comprehensive processing, display and analysis for in vivo MR spectroscopic imaging. NMR Biomed. 19, 492–503. http://dx.doi.org/10.1002/nbm.1025.

Mlynárik, V., Cudalbu, C., Clément, V., Marino, D., Radovanovic, I., Gruetter, R., 2012. In vivo metabolic profiling of glioma-initiating cells using proton magnetic resonance spectroscopy at 14.1 Tesla. NMR Biomed. 25, 506–513. http://dx.doi.org/10.1002/nbm.1763.

Naressi, A., Couturier, C., Devos, J.M., Janssen, M., Mangeat, C., de Beer, R., Graveron-Demilly, D., 2001. Java-based graphical user interface for the MRUI quantitation package. MAGMA 12, 141–152.

Ogg, R.J., Kingsley, P.B., Taylor, J.S., 1994. WET, a T_1- and B_1-insensitive water-suppression method for in vivo localized ^{1}H NMR spectroscopy. J. Magn. Reson. B 104, 1–10.

Opstad, K.S., Murphy, M.M., Wilkins, P.R., Bell, B.A., Griffiths, J.R., Howe, F.A., 2004. Differentiation of metastases from high-grade gliomas using short echo time ^{1}H spectroscopy. J. Magn. Reson. Imaging 20, 187–192. http://dx.doi.org/10.1002/jmri.20093.

Penner, J., Bartha, R., 2014. Semi-LASER ^{1}H MR spectroscopy at 7 Tesla in human brain: metabolite quantification incorporating subject-specific macromolecule removal. Magn. Reson. Med. http://dx.doi.org/10.1002/mrm.25380.

Pfeuffer, J., Tkác, I., Provencher, S.W., Gruetter, R., 1999. Toward an in vivo neurochemical profile: quantification of 18 metabolites in short-echo-time ^{1}H NMR spectra of the rat brain. J. Magn. Reson. 141, 104–120. http://dx.doi.org/10.1006/jmre.1999.1895.

Pouwels, P.J.W., Frahm, J., 1998. Regional metabolite concentrations in human brain as determined by quantitative localized proton MRS. Magn. Reson. Med. 39, 53–60. http://dx.doi.org/10.1002/mrm.1910390110.

Považan, M., Strasser, B., Hangel, G., Chmelik, M., Gruber, S., Trattnig, S., Bogner, W., 2014. Automated routine for MRSI data processing. 2nd TRANSACT Meeting—Quality Issues in Clinical MR Spectroscopy. University and Inselspital Bern, Switzerland, p. S2.

Provencher, S.W., 2001. Automatic quantitation of localized in vivo ^{1}H spectra with LCModel. NMR Biomed. 14, 260–264.

Saunders, D.E., Howe, F.A., van den Boogaart, A., Griffiths, J.R., Brown, M.M., 1997. Discrimination of metabolite from lipid and macromolecule resonances in cerebral infarction in humans using short echo proton spectroscopy. J. Magn. Reson. Imaging 7, 1116–1121.

Schaller, B., Xin, L., Cudalbu, C., Gruetter, R., 2013. Quantification of the neurochemical profile using simulated macromolecule resonances at 3 T. NMR Biomed. 26, 593–599. http://dx.doi.org/10.1002/nbm.2896.

Schaller, B., Xin, L., Gruetter, R., 2014. Is the macromolecule signal tissue-specific in healthy human brain? A ^{1}H MRS study at 7 tesla in the occipital lobe. Magn. Reson. Med. 72, 1–7. http://dx.doi.org/10.1002/mrm.24995.

Seeger, U., Mader, I., Nägele, T., Grodd, W., Lutz, O., Klose, U., 2001. Reliable detection of macromolecules in single-volume ^{1}H NMR spectra of the human brain. Magn. Reson. Med. 45, 948–954.

Seeger, U., Klose, U., Mader, I., Grodd, W., Nägele, T., 2003. Parameterized evaluation of macromolecules and lipids in proton MR spectroscopy of brain diseases. Magn. Reson. Med. 49, 19–28. http://dx.doi.org/10.1002/mrm.10332.

Smith, S.M., 2002. Fast robust automated brain extraction. Hum. Brain Mapp. 17, 143–155. http://dx.doi.org/10.1002/hbm.10062.

Snoussi, K., Gillen, J.S., Horska, A., Puts, N. a J., Pradhan, S., Edden, R. a E., Barker, P.B., 2014. Comparison of brain gray and white matter macromolecule resonances at 3 and 7 Tesla. Magn. Reson. Med. 00, 1–7. http://dx.doi.org/10.1002/mrm.25468.

Strasser, B., Chmelik, M., Robinson, S.D., Hangel, G., Gruber, S., Trattnig, S., Bogner, W., 2013. Coil combination of multichannel MRSI data at 7 T: MUSICAL. NMR Biomed. 26, 1796–1805. http://dx.doi.org/10.1002/nbm.3019.

Thomas, M.A., Yue, K., Binesh, N., Davanzo, P., Kumar, A., Siegel, B., Frye, M., Curran, J., Lufkin, R., Martin, P., Guze, B., 2001. Localized two-dimensional shift correlated MR spectroscopy of human brain. Magn. Reson. Med. 46, 58–67. http://dx.doi.org/10.1002/mrm.1160.

Tkáč, I., Andersen, P., Adriany, G., Merkle, H., Ugurbil, K., Gruetter, R., 2001. In vivo ^{1}H NMR spectroscopy of the human brain at 7 T. Magn. Reson. Med. 46, 451–456. http://dx.doi.org/10.1016/j.jmr.2010.06.006.

Tkáč, I., Oz, G., Adriany, G., Uğurbil, K., Gruetter, R., 2009. In vivo ^{1}H NMR spectroscopy of the human brain at high magnetic fields: metabolite quantification at 4 T vs. 7 T. Magn. Reson. Med. 62, 868–879. http://dx.doi.org/10.1002/mrm.22086.

Vanhamme, L., van den Boogaart, A., Van Huffel, S., 1997. Improved method for accurate and efficient quantification of MRS data with use of prior knowledge. J. Magn. Reson. 129, 35–43. http://dx.doi.org/10.1006/jmre.1997.1244.

Xin, L., Gambarota, G., Mlynárik, V., Gruetter, R., 2008. Proton T_2 relaxation time of J-coupled cerebral metabolites in rat brain at 9.4 T. NMR Biomed. 21, 396–401. http://dx.doi.org/10.1002/nbm.1205.

Xin, L., Schaller, B., Mlynarik, V., Lu, H., Gruetter, R., 2013. Proton T_1 relaxation times of metabolites in human occipital white and gray matter at 7 T. Magn. Reson. Med. 69, 931–936. http://dx.doi.org/10.1002/mrm.24352.

Zhang, Y., Gabr, R.E., Schär, M., Weiss, R.G., Bottomley, P.A., 2012. Magnetic resonance spectroscopy with linear algebraic modeling (SLAM) for higher speed and sensitivity. J. Magn. Reson. 218, 66–76. http://dx.doi.org/10.1016/j.jmr.2012.03.008.